

Spectral function of Fermi polarons at finite temperature from a self-consistent many-body T -matrix approach in real frequency

Hui Hu^{*} and Xia-Ji Liu[†]*Centre for Quantum Technology Theory, Swinburne University of Technology, Melbourne 3122, Australia*

(Received 20 November 2023; revised 17 May 2024; accepted 20 May 2024; published 6 June 2024)

We theoretically examine the finite-temperature spectral function of Fermi polarons in three dimensions by using a self-consistent many-body T -matrix theory in real frequency. In comparison with the previous results from a non-self-consistent many-body T -matrix approach, we show that the treatment of self-consistency in the impurity Green's function leads to notable changes in almost all the dynamical quantities, including the vertex function, impurity self-energy, and spectral function. Eventually, it gives rise to quantitatively different predictions for the measurable radio-frequency spectrum and Raman spectrum at finite temperature. Using the recent spectroscopic measurements as a benchmark, we find that the self-consistent many-body T -matrix theory somehow provides a better explanation for the experimental data. The notable difference in the predictions from the non-self-consistent and self-consistent theories suggests that more accurate theoretical descriptions are needed in order to fully account for the current spectroscopic observations on Fermi polarons.

DOI: [10.1103/PhysRevA.109.063313](https://doi.org/10.1103/PhysRevA.109.063313)

I. INTRODUCTION

The Fermi polaron, an impurity interacting with a noninteracting Fermi sea of fermions, is probably the oldest and simplest quantum many-body system that plays a significant role in our understanding of many-particle physics [1,2]. Recent rapid experimental advances in cold-atom research have brought renewed interest in the Fermi-polaron problem [3–8] due to the unprecedented tunability in interparticle interaction, purity, and dimensionality [9,10]. As a consequence, the physics of Fermi polarons can now be experimentally explored in a quantitative manner with atomic Fermi-Fermi mixtures or Bose-Fermi mixtures near Feshbach resonances, in which in the dilute limit minority fermionic or bosonic atoms act as independent, uncorrelated impurities [4,5].

Spectroscopic measurements, such as radio-frequency (rf) spectroscopy [4,11–15], Ramsey interferometry [14,16], and, most recently, Raman spectroscopy [17], provide useful tools for revealing a number of intriguing features of Fermi polarons. To date, polaron energy has been measured with various spectroscopies with excellent accuracy and has been well explained by existing theories based on the variational Chevy ansatz [3,18–22], diagrammatic many-body T -matrix approximations [23–32], and quantum Monte Carlo simulations [33–35]. The dynamical properties concerning the measured spectroscopy line shape, however, are less understood. In particular, the spectral function of Fermi polarons, which is the fundamental quantity that determines rf spectroscopy and Raman spectroscopy, is notoriously difficult to accurately predict.

Pioneering quantum Monte Carlo simulations of the spectral function were attempted by Gouliko and her collaborators [36]. However, the accuracy needed to be improved. Exact numerical calculations are available in the heavy-polaron limit of infinitely large impurity mass [37–39]. However, the experimental realization of heavy Fermi polarons remains to be demonstrated. Current knowledge of the polaron spectral function largely relies on a non-self-consistent many-body T -matrix theory [25,27–32] or its equivalent form of the variational Chevy ansatz [20,21], both at zero temperature and finite temperature. In the non-self-consistent T -matrix theory, the successive scatterings between the impurity and Fermi sea are taken into account in the form of ladder diagrams, whose contributions can be diagrammatically calculated by using the bare, noninteracting impurity Green's function [23,29].

The purpose of this work is to calculate the spectral function of Fermi polarons based on a self-consistent many-body T -matrix theory, in which the contributions from ladder diagrams are self-consistently calculated by using a dressed, interacting impurity Green's function. A similar theoretical investigation was presented earlier by Tajima and his coworkers [28], in which numerical calculations were carried out with imaginary-time Green's functions to avoid numerical instability. We improve their interesting work by using real-time Green's functions. This may remove potential errors due to the uncontrollable numerical analytic continuation applied to convert the imaginary frequency to the real frequency, which is known to be ill defined [36].

We observe that the non-self-consistent and self-consistent theories lead to quantitatively different predictions for the spectral function of Fermi polarons. As a result, the predicted rf spectrum and Raman spectrum also differ quantitatively. In comparison with the most recent spectroscopic measurements [15,17], neither prediction can explain the experimental data in a satisfactory way, although the self-consistent results seem

*hhu@swin.edu.au

†xiajiliu@swin.edu.au

to provide slightly better agreement. The discrepancy between theories and experiments emphasizes the importance of developing a more accurate theoretical framework for Fermi polarons.

It should be noted that, in perturbative diagrammatic theories, the advantage of considering self-consistency in Feynman diagrams is not taken for granted, particularly in the strongly interacting regime that we are exploring [40–42]. For example, for a strong-interacting balanced spin-1/2 Fermi gas with an equal-spin population, both the non-self-consistent and self-consistent many-body T -matrix theories have been used to calculate the spectral function of a unitary Fermi gas with infinitely large scattering length at the Feshbach resonance [43–46]. However, debates about the accuracy of both calculations are unsettled since they lead to entirely different predictions on the existence of pair-fluctuation-induced pseudogap [47,48]. A possible source for this qualitative discrepancy may arise from the errors in numerical analytic continuation adopted in the self-consistent T -matrix calculations [45]. It would be interesting to remove such avoidable errors in the self-consistent theory by extending our work to directly calculate the spectral function of the unitary Fermi gas in the real frequency.

The rest of this paper is organized as follows. In Sec. II, we outline the model Hamiltonian for Fermi polarons and briefly summarize the self-consistent many-body T -matrix approach. We emphasize how to realize the numerical procedure for self-consistency of the impurity Green's function with the real frequency. In Sec. III, we discuss the vertex function, the impurity self-energy, and the polaron spectral function and show the changes in these quantities because of our self-consistent treatment. We also present the temperature dependence of the polaron energy and decay rate. In Sec. IV, we calculate the rf spectrum and Raman spectrum. We compare the theoretical results, predicted by both non-self-consistent and self-consistent many-body T -matrix theories, with the experimental data. The conclusions and outlook follow in Sec. V.

II. MODEL HAMILTONIAN AND SELF-CONSISTENT MANY-BODY T -MATRIX APPROACH

As in the experiments [4,14,15,17], we consider a highly imbalanced spin-1/2 Fermi gas of ultracold atoms with equal mass m near an s -wave Feshbach resonance, distributed uniformly in volume V in three dimensions. In the limit of vanishing density of minority atoms, we treat them as uncorrelated impurities, interacting with a noninteracting Fermi sea of majority atoms via a contact interaction potential $g\delta(\mathbf{r} - \mathbf{r}')$. Here, g is the bare interaction strength that has to be replaced by the s -wave scattering length a using the standard relation

$$\frac{1}{g} = \frac{m}{4\pi\hbar^2 a} - \frac{1}{V} \sum_{\mathbf{k}} \frac{m}{\hbar^2 \mathbf{k}^2}, \quad (1)$$

so the ultraviolet divergence inherent in the contact potential can be effectively regularized. The system under consideration is well described by a single-channel model Hamiltonian,

$$\mathcal{H} = \sum_{\mathbf{k}} \epsilon_{\mathbf{k}} c_{\mathbf{k}}^{\dagger} c_{\mathbf{k}} + \sum_{\mathbf{k}} \epsilon_{\mathbf{k}} d_{\mathbf{k}}^{\dagger} d_{\mathbf{k}} + g \sum_{\mathbf{q}\mathbf{k}\mathbf{k}'} c_{\mathbf{k}}^{\dagger} d_{\mathbf{q}-\mathbf{k}}^{\dagger} d_{\mathbf{q}-\mathbf{k}'} c_{\mathbf{k}'}, \quad (2)$$

where $c_{\mathbf{k}}^{\dagger}$ ($c_{\mathbf{k}}$) and $d_{\mathbf{k}}^{\dagger}$ ($d_{\mathbf{k}}$) are the creation (annihilation) field operators for fermionic atoms and the impurity, respectively. For clarity, we have suppressed the volume V in the model Hamiltonian, so the integration over the momentum $\sum_{\mathbf{k}}$ in the following should be always understood as $(1/V) \sum_{\mathbf{k}} = \int d\mathbf{k}/(2\pi)^3$. The first two terms in the Hamiltonian describe the kinetic, noninteracting part with the dispersion relation $\epsilon_{\mathbf{k}} = \hbar^2 \mathbf{k}^2/(2m)$, and the last term describes the interaction between the impurity and the Fermi sea. The chemical potentials are not specified in the Hamiltonian, but it should be understood that the number n of fermions in the Fermi sea is tuned by a chemical potential μ ; i.e., we will modify the single-particle dispersion relation to $\xi_{\mathbf{k}} = \epsilon_{\mathbf{k}} - \mu = \hbar^2 \mathbf{k}^2/(2m) - \mu$. Moreover, for a single impurity, it is not necessary to explicitly introduce an impurity chemical potential [23,29]. Throughout this work, we take the Fermi wave vector $k_F = (6\pi^2 n)^{1/3}$ and the Fermi energy $\epsilon_F = \hbar^2 k_F^2/(2m)$ as the units of the wave vector k (or q) and of the energy (or frequency), respectively.

A. Many-body T -matrix theories

We solve the model Hamiltonian by using the many-body T -matrix theories, which are well-documented in the literature [23,24,28,29]. Here, we summarize only the key equations, which are relevant to address the self-consistency of the impurity Green's function that we wish to focus on in this work.

In the many-body T -matrix approximation, one keeps track on ladder diagrams, which represent the successive forward scatterings between the impurity and fermions in the particle-particle channel. At a nonzero temperature T , the contributions of ladder diagrams are represented by the inverse two-particle vertex function,

$$\Gamma^{-1}(\mathbf{q}, \omega) = \frac{1}{g} - \sum_{\mathbf{k}} f(-\xi_{\mathbf{q}-\mathbf{k}}) G(\mathbf{k}, \omega - \xi_{\mathbf{q}-\mathbf{k}}), \quad (3)$$

where $f(x) \equiv 1/(e^{\beta x} + 1)$, with $\beta \equiv 1/(k_B T)$, is the Fermi-Dirac distribution function and $G(\mathbf{k}, \omega)$ is the retarded impurity Green's function at momentum \mathbf{k} with real frequency ω at finite temperature. In our self-consistent treatment, this impurity Green's function itself already includes the interaction effect. In other words, it is a *dressed* Green's function given by the Dyson equation,

$$G(\mathbf{k}, \omega) = \frac{1}{\omega - \epsilon_{\mathbf{k}} - \Sigma(\mathbf{k}, \omega)}, \quad (4)$$

where the retarded impurity self-energy $\Sigma(\mathbf{k}, \omega)$ is related to the vertex function $\Gamma(\mathbf{q}, \omega)$,

$$\Sigma(\mathbf{k}, \omega) = \sum_{\mathbf{q}} f(\xi_{\mathbf{q}-\mathbf{k}}) \Gamma(\mathbf{q}, \omega + \xi_{\mathbf{q}-\mathbf{k}}). \quad (5)$$

Equations (3), (4) and (5) provide a set of coupled equations in the real-frequency domain, where the dressed impurity Green's function $G(\mathbf{k}, \omega)$ needs to be self-consistently determined.

In the non-self-consistent T -matrix theory, such self-consistency is not required. In Eq. (3), we directly use the noninteracting Green's function $G_0(\mathbf{k}, \omega - \xi_{\mathbf{q}-\mathbf{k}}) =$

$1/(\omega - \xi_{\mathbf{q}-\mathbf{k}} - \epsilon_{\mathbf{k}})$ to replace the dressed Green's function $G(\mathbf{k}, \omega - \xi_{\mathbf{q}-\mathbf{k}})$, yielding the expression [23]

$$\Gamma_0^{-1}(\mathbf{q}, \omega) = \frac{m}{4\pi\hbar^2 a} - \sum_{\mathbf{k}} \left[\frac{1 - f(\xi_{\mathbf{q}-\mathbf{k}})}{\omega - \xi_{\mathbf{q}-\mathbf{k}} - \epsilon_{\mathbf{k}}} + \frac{m}{\hbar^2 \mathbf{k}^2} \right], \quad (6)$$

where we have rewritten the bare interaction strength g in terms of the physical s -wave scattering length a . In turn, we substitute the leading-order approximated vertex function $\Gamma_0(\mathbf{q}, \omega)$ into Eq. (5) to determine the impurity self-energy $\Sigma_0(\mathbf{k}, \omega)$ at the *first* iteration. In the non-self-consistent treatment, we simply assume that the resulting self-energy $\Sigma_0(\mathbf{k}, \omega)$ might already be useful enough and would lead to a reasonably accurate impurity Green's function $G(\mathbf{k}, \omega)$ when it is used in the Dyson equation (4).

In contrast, in our fully self-consistent treatment, we need to use $\Sigma_0(\mathbf{k}, \omega)$ to obtain an improved impurity Green's function $G_1(\mathbf{k}, \omega - \xi_{\mathbf{q}-\mathbf{k}}) = 1/[\omega - \xi_{\mathbf{q}-\mathbf{k}} - \epsilon_{\mathbf{k}} - \Sigma_0(\mathbf{k}, \omega - \xi_{\mathbf{q}-\mathbf{k}})]$ and then repeat the above-mentioned procedure to iteratively update the impurity Green's function until it converges.

$$\delta\chi(\mathbf{q}, \omega) \equiv \Gamma^{-1}(\mathbf{q}, \omega) - \Gamma_0^{-1}(\mathbf{q}, \omega) = - \sum_{\mathbf{k}} \frac{f(-\xi_{\mathbf{q}-\mathbf{k}})\Sigma(\mathbf{k}, \omega - \xi_{\mathbf{q}-\mathbf{k}})}{(\omega - \xi_{\mathbf{q}-\mathbf{k}} - \epsilon_{\mathbf{k}})[\omega - \xi_{\mathbf{q}-\mathbf{k}} - \epsilon_{\mathbf{k}} - \Sigma(\mathbf{k}, \omega - \xi_{\mathbf{q}-\mathbf{k}})]} \quad (7)$$

would be small and therefore would not require high-precision calculation. We may then artificially introduce a small imaginary part η to the real frequency ω to remove the singularity in the integrand of Eq. (7). In practice, we find that the approximated expression

$$\delta\chi(\mathbf{q}, \omega) \simeq 2\delta\chi(\mathbf{q}, \omega + i\eta) - \delta\chi(\mathbf{q}, \omega + 2i\eta) \quad (8)$$

works extremely well, with a small $\eta = 0.2\epsilon_F$. The choice of this value for η is carefully examined in Appendix A. We confirm that the converged results of the impurity Green's function and spectral function do not depend on η .

The whole procedure of numerical iterations is then simple to carry out. We start from the non-self-consistent result of the self-energy $\Sigma_0(\mathbf{k}, \omega)$ and calculate the difference $\delta\chi(\mathbf{q}, \omega)$ using Eqs. (7) and (8). We then update the vertex function

$$\Gamma(\mathbf{q}, \omega) = \frac{1}{\Gamma_0^{-1}(\mathbf{q}, \omega) + \delta\chi(\mathbf{q}, \omega)} \quad (9)$$

and use it to obtain a new self-energy $\Sigma(\mathbf{k}, \omega)$ with Eq. (5). The iteration is repeated until the change $\delta\Sigma(\mathbf{k}, \omega)$ in the self-energy becomes negligible. Typically, the convergence can quickly be reached in just a few iterations. During the iteration procedure, the self-energy $\Sigma(\mathbf{k}, \omega)$ will be stored in the form of a two-dimensional array. The numbers of grid points for the momentum $k = |\mathbf{k}|$ and the frequency ω are about 200 and 500, respectively. The dense grid points are distributed in a nonequidistant way, so both large-momentum and large-frequency behaviors of the self-energy can be well sampled. We can then use a cubic spline interpolation to accurately extract a self-energy $\Sigma(\mathbf{k}, \omega)$ at arbitrary momentum k and frequency ω .

It is also worth noting that, for a large and positive dimensionless interaction parameter $1/(k_F a)$, the vertex function $\Gamma(\mathbf{q}, \omega)$ may develop a pole, which signals the existence of

The numerical workload of self-consistent calculations is therefore much heavier.

B. Numerical calculations

To reduce the workload, it is worth noting that the key difficulty of numerical calculations comes from the integration over the momentum \mathbf{k} in Eq. (3) because the poles of the impurity Green's function make the integrand very singular. This singularity actually already appears in the non-self-consistent calculations. As can be readily seen from Eq. (6), the integrand on the right-hand side badly diverges at some momenta \mathbf{k} once the frequency ω is in the two-particle continuum and satisfies $\omega = \xi_{\mathbf{q}-\mathbf{k}} + \epsilon_{\mathbf{k}}$. Fortunately, since we can precisely locate the pole position of the noninteracting impurity Green's function, the vertex function $\Gamma_0(\mathbf{q}, \omega)$ can be efficiently calculated, as outlined in detail in a previous work [29]. As we anticipate that $\Gamma_0(\mathbf{q}, \omega)$ makes the dominant contribution to the full vertex function $\Gamma(\mathbf{q}, \omega)$, the difference

a well-defined molecule state [23]. In that case, specific attention should be paid to handling the singularity in Eq. (5). However, in this work, we always focus on the polaron regime, where the vertex function $\Gamma(\mathbf{q}, \omega)$ is consistently well behaved. Although the initial vertex function $\Gamma_0(\mathbf{q}, \omega)$ may suffer from a singularity at large $1/(k_F a)$ in the polaron regime, the singularity will quickly be removed by the self-consistency iteration.

III. POLARON SPECTRAL FUNCTION

In Fig. 1, we report the zero-momentum vertex function at two interaction parameters and at a low temperature $T = 0.2T_F$, predicted by the self-consistent (black solid lines) and non-self-consistent (red dashed lines) many-body T -matrix theories. In Figs. 1(a) and 1(b), we take the unitary limit $1/(k_F a) = 0$, where a two-body bound state starts to emerge. In Figs. 1(c) and 1(d), we consider the Bose-Einstein condensate (BEC) side or the molecule side of the Feshbach resonance with $1/(k_F a) = 0.5$, where a two-body bound state exists, with binding energy $E_B = 2\epsilon_F/(k_F a)^2 = 0.5\epsilon_F$. For both interaction parameters, we find that the self-consistency treatment strongly modifies the results of the vertex function.

Let us focus on the imaginary part of the vertex function shown in Figs. 1(b) and 1(d). Physically, the vertex function describes a molecule state in the presence of the many-body environment of a Fermi sea [33]. Its imaginary part can therefore be used to define a molecule spectral function,

$$A_{\text{mol}}(\mathbf{q}, \omega) \propto -\frac{1}{\pi} \text{Im}\Gamma(\mathbf{q}, \omega), \quad (10)$$

which is precisely the quantity plotted. We always find a peak in $A_{\text{mol}}(\mathbf{q}, \omega)$, although there is no well-defined two-body

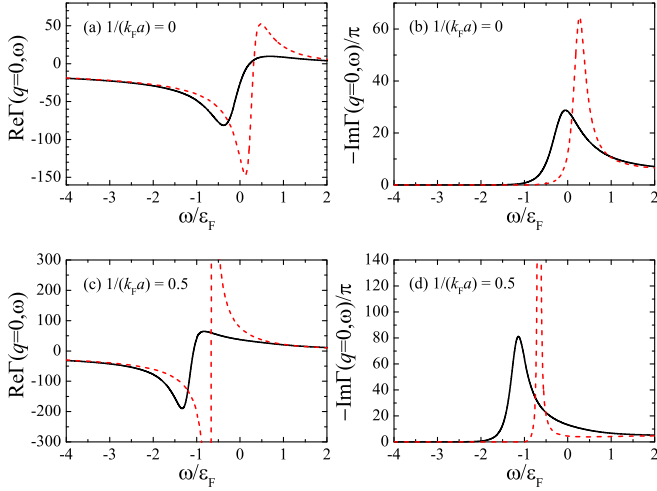


FIG. 1. (a) and (c) The real part and (b) and (d) imaginary part of the zero-momentum vertex function $\Gamma(q = 0, \omega)$, in arbitrary units, at temperature $T = 0.2T_F$. The top panels are the results in the unitary limit [i.e., $1/(k_F a) = 0$], while the bottom panels present the results on the molecular side of the Feshbach resonance with $1/(k_F a) = 0.5$. The black solid lines and the red dashed lines correspond to the predictions from the self-consistent and non-self-consistent many-body T -matrix theories, respectively.

bound state in the unitary limit. This is understandable since the presence of a Fermi sea is known to be favorable for stabilizing a many-body (Cooper) pair [49]. It is easy to see that the non-self-consistent T -matrix theory predicts a much sharper peak in the molecule spectral function than the self-consistent T -matrix theory. Moreover, with the self-consistency in the impurity Green's function, the molecule peak shifts to the low-energy side by an amount about $0.5\varepsilon_F$.

Although for the impurity Green's function the advantage of taking the self-consistency is not granted, for the vertex function (or, boldly, the molecule Green's function), there is no doubt that the self-consistency treatment will improve its accuracy. The lower molecule peak or smaller molecule energy, predicted by the self-consistent T -matrix theory, therefore implies that the critical interaction strength for the polaron-molecule transition [50] can be smaller than what is predicted by the non-self-consistent T -matrix theory. This observation is consistent with previous T -matrix studies on polaron energy at zero temperature [24].

In Fig. 2, we present the real part and the imaginary part of the impurity self-energy at zero momentum for the same parameters as in Fig. 1. Once again, we find significant changes due to the self-consistency treatment. At $k = 0$, the pole of the impurity Green's function in Eq. (4) occurs at $\omega = \text{Re}\Sigma(k = 0, \omega)$ if we neglect the (possibly large) imaginary part $\text{Im}\Sigma(k = 0, \omega)$. Therefore, in Figs. 2(a) and 2(c), we also show the curve $y = \omega$ by a green dotted line. The crossing point between the green dotted line and the curve $\text{Re}\Sigma(k = 0, \omega)$ determines the polaron energy \mathcal{E}_P at the pole of the impurity Green's function.

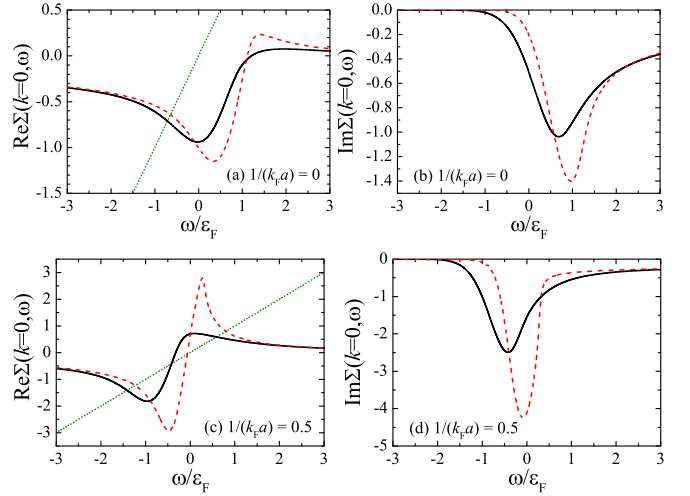


FIG. 2. (a) and (c) The real part and (b) and (d) imaginary part of the zero-momentum self-energy $\Sigma(k = 0, \omega)$, in units of ε_F , at temperature $T = 0.2T_F$ and at the two interaction strengths indicated. The black solid lines and the red dashed lines correspond to the predictions from the self-consistent and non-self-consistent many-body T -matrix theories, respectively. In (a) and (c), the crossing points of $\text{Re}\Sigma(k = 0, \omega)$ and the green dotted curves (i.e., $y = \omega$) determine the polaron energies (of different polaron branches).

On the negative-frequency side, we always find a crossing point, which gives the energy of an attractive Fermi polaron. The self-consistent many-body T -matrix theory predicts a lower polaron energy than its non-self-consistent counterpart, with an energy shift of about $0.1\varepsilon_F - 0.2\varepsilon_F$, which is smaller than the shift in the molecule energy that we observe in the molecule spectral function. On the other hand, on the positive-frequency side, we can find only the crossing point at the positive interaction parameter $1/(k_F a) > 0$ in Fig. 2(c), which determines the energy of the repulsive Fermi polaron. As in the case of the attractive polaron, we observe that the self-consistency still leads to a small redshift in the repulsive-polaron energy. Interestingly, at $1/(k_F a) = 0.5$ there is an additional crossing point located close to the zero frequency $\omega = 0$. However, this crossing point can hardly be viewed as the pole of the impurity Green's function since the imaginary part of the impurity self-energy becomes too large near $\omega = 0$.

For the imaginary part of the impurity self-energy shown in Figs. 2(b) and 2(d), we find that the self-consistent T -matrix theory consistently predicts a more negative imaginary part than the non-self-consistent T -matrix theory at the frequency near the polaron energy. As we shall see, it will lead to the prediction of a larger decay rate of polaron quasiparticles.

We now turn to discussing the impurity spectral function defined by

$$A(\mathbf{k}, \omega) = -\frac{1}{\pi} \text{Im}G(\mathbf{k}, \omega). \quad (11)$$

Near the polaron energy \mathcal{E}_P at the pole of the impurity Green's function, we may Taylor expand the self-energy at small

momentum,

$$\Sigma(\mathbf{k} \rightarrow \mathbf{0}, \omega \rightarrow \mathcal{E}_p) \simeq \mathcal{E}_p + \left. \frac{\partial \text{Re}\Sigma(\mathbf{k}, \mathcal{E}_p)}{\partial \epsilon_{\mathbf{k}}} \right|_{\mathbf{k}=\mathbf{0}} \epsilon_{\mathbf{k}} + \left. \frac{\partial \text{Re}\Sigma(0, \omega)}{\partial \omega} \right|_{\omega=\mathcal{E}_p} (\omega - \mathcal{E}_p) + i \text{Im}\Sigma(0, \mathcal{E}_p), \quad (12)$$

where we have used the condition $\mathcal{E}_p = \text{Re}\Sigma(0, \mathcal{E}_p)$. It is a convention to introduce the polaron residue

$$\mathcal{Z} = \left[1 - \left. \frac{\partial \text{Re}\Sigma(\mathbf{0}, \omega)}{\partial \omega} \right|_{\omega=\mathcal{E}_p} \right]^{-1} \quad (13)$$

and polaron decay rate

$$\Gamma = -2\mathcal{Z} \text{Im}\Sigma(\mathbf{0}, \mathcal{E}_p), \quad (14)$$

with which we may explicitly rewrite the zero-momentum spectral function $A(k=0, \omega)$ into the approximate Lorentzian form near the polaron energy,

$$A(0, \omega) \simeq \mathcal{Z} \frac{\Gamma/(2\pi)}{(\omega - \mathcal{E}_p)^2 + \Gamma^2/4}. \quad (15)$$

Therefore, the residue \mathcal{Z} measures the area under the polaron peak, and the decay rate Γ determines the FWHM of the peak.

In Fig. 3, we report the zero-momentum impurity spectral function at three typical temperatures in the unitary limit

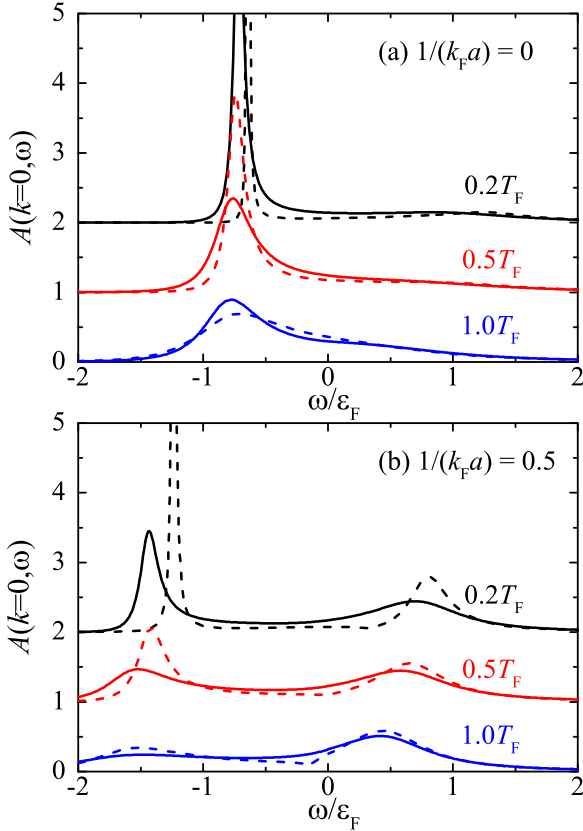


FIG. 3. Zero-momentum spectral function of the impurity (in units of ϵ_F^{-1}) (a) in the unitary limit and (b) on the molecular side of the Feshbach resonance at three different temperatures, as indicated. For clarity, the results at $T = 0.2T_F$ and $T = 0.5T_F$ are vertically upshifted. The solid lines (dashed lines) show the predictions of the self-consistent (non-self-consistent) many-body T -matrix theory.

with $1/(k_F a) = 0$ [Fig. 3(a)] and on the BEC side of the Feshbach resonance with $1/(k_F a) = 0.5$ [Fig. 3(b)]. In comparison with the non-self-consistent T -matrix theoretical results (i.e., red dashed lines), it is readily seen that the self-consistent T -matrix theory always predicts a broader polaron peak, indicating a larger polaron decay rate. The temperature evolutions of the polaron spectral function provided by the two T -matrix theories are qualitatively similar. However, there are quantitative differences that we shall discuss in detail in the following.

In the unitary limit [Fig. 3(a)], both T -matrix theories show a nonmonotonic temperature dependence of the (attractive) polaron energy. This can be seen more clearly in Fig. 4, where we report the polaron energy and decay rate as a function of the temperature. With increasing temperature, the polaron energy initially decreases, reaches a global minimum at certain temperature, and then increases. The initial decrease in the polaron energy with temperature might be understood from the Pauli exclusion principle. The thermal blurring of the Fermi sea reduces the statistical exclusion and therefore is favorable for the particle-hole excitations that are crucial for the polaron formation [15]. However, a large temperature eventually reduces the effective interaction between the

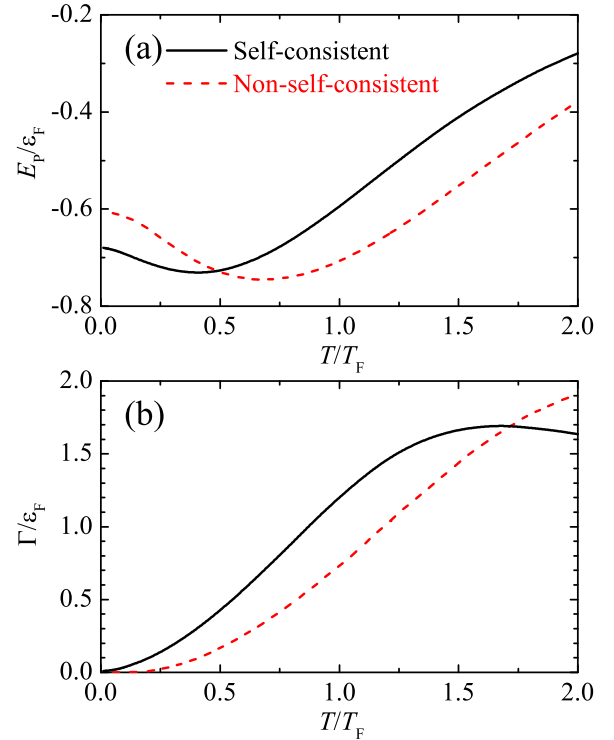


FIG. 4. Temperature dependence of (a) the energy and (b) decay rate of the attractive polaron in the unitary limit. The black solid lines and red dashed lines report the predictions of the self-consistent and non-self-consistent many-body T -matrix theories, respectively.

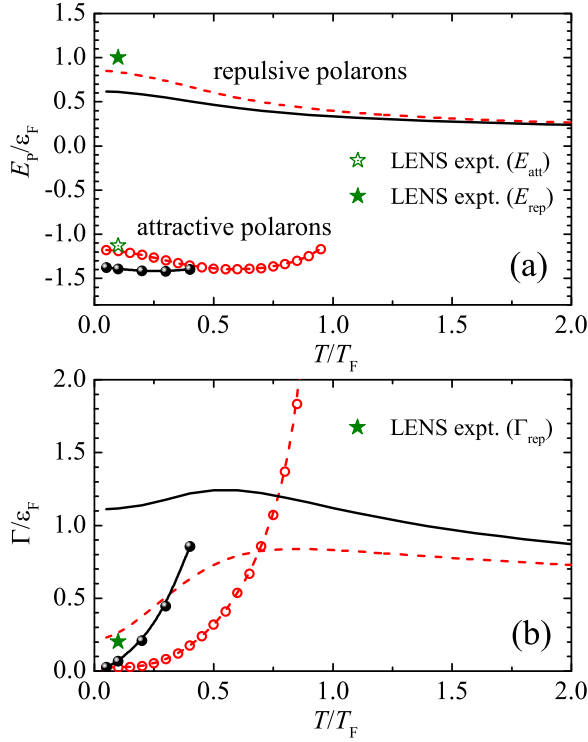


FIG. 5. Temperature dependence of (a) the energy and (b) decay rate of the attractive polaron and repulsive polaron at interaction strength $1/(k_F a) = 0.5$. The black solid lines and red dashed lines respectively report the predictions of the self-consistent and non-self-consistent many-body T -matrix theories for the repulsive polaron. The black solid lines with solid circles and red dashed lines with open circles correspond to the results of the attractive polaron. The green stars show the experimental data for the energy and decay rate of the attractive polaron (empty star) and of the repulsive polaron (solid stars) at $T \simeq 0.1T_F$, extracted from Ref. [14].

impurity and Fermi sea and increases the polaron energy. We find that the two many-body T -matrix theories give different temperatures for the minimum polaron energy, so the two curves for the polaron energy cross at around $T_X \sim 0.5T_F$. Above T_X , the self-consistent T -matrix theory predicts a larger polaron energy than the non-self-consistent T -matrix theory, different from what we observe in Fig. 2 for the impurity self-energy at $T = 0.2T_F$.

On the BEC side of the Feshbach resonance [see Fig. 3(b)], there are two branches of Fermi polarons. In Fig. 5, we show the temperature dependence of the polaron energy and decay rate for both the attractive Fermi polaron and repulsive Fermi polaron. The attractive-polaron branch does not always exist. We can find the attractive-polaron solution only for $\mathcal{E}_p = \text{Re}\Sigma(0, \mathcal{E}_p)$ at temperature $T < 0.5T_F$ in the self-consistent many-body T -matrix theory. The non-self-consistent theory seems to give a wider temperature range for the attractive polaron, i.e., $T < T_F$. However, its decay rate increases too rapidly with temperature. As a result, it may hardly be viewed as a well-defined quasiparticle once $T > 0.7T_F$, where the decay rate becomes larger than ϵ_F .

In contrast, we can always find a solution of $\mathcal{E}_p = \text{Re}\Sigma(0, \mathcal{E}_p)$ for the repulsive-polaron branch. The

repulsive-polaron energies predicted by the two theories do not differ too much. The difference is about $0.3\epsilon_F$ at most near zero temperature, and it becomes negligible above the Fermi degenerate temperature. Remarkably, the decay rates of the repulsive polaron given by the two T -matrix theories are very different. In particular, near zero temperature the decay rate obtained from the self-consistent calculations is about $1.1\epsilon_F$, significantly larger than the non-self-consistent result of about $0.2\epsilon_F$. In comparison with the recent measurement from the European Laboratory for Non-Linear Spectroscopy (LENS), the decay rate of the repulsive polaron calculated from the non-self-consistent T -matrix theory agrees better with the experimental data [see, i.e., the green star in Fig. 5(b) at $T \simeq 0.1T_F$], which are tens of percent of the Fermi energy [14]. We note finally that the repulsive-polaron energy from both T -matrix theories decreases with increasing temperature. The temperature dependence of the repulsive-polaron decay rate from both theories is not monotonic. Once $T > 0.7T_F$, the polaron decay rate becomes comparable to ϵ_F . The repulsive polaron may then hardly be treated as a well-defined quasiparticle as the quality factor $Q = \mathcal{E}_p/\Gamma < 1$.

IV. ATOMIC SPECTROSCOPY

In experiments, the polaron spectral function can be probed by using rf spectroscopy or Raman spectroscopy. In those spectroscopic measurements, the impurity is initially in the hyperfine state that interacts with the Fermi sea. It is then transferred or ejected to a second, noninteracting hyperfine state using either rf beams or Raman beams with energy ω . According to the linear-response theory the ejection rate is proportional to [15,17,29,32]

$$I(\omega) = \frac{1}{V} \sum_{\mathbf{k}} A[\mathbf{k}, \epsilon_{\mathbf{k}+\mathbf{Q}} - \omega] f(\epsilon_{\mathbf{k}+\mathbf{Q}} - \omega - \mu_I), \quad (16)$$

where \mathbf{Q} is the momentum of the light beams. In the case of rf spectroscopy, the momentum is negligible, so we take $\mathbf{Q} = 0$. Realistically, one always uses a small impurity density n_{imp} in the experiments [15,17], which can be theoretically set by an impurity chemical potential μ_I through the number equation,

$$n_{\text{imp}} = \frac{1}{V} \sum_{\mathbf{k}} \int_{-\infty}^{+\infty} d\omega f(\omega - \mu_I) A(\mathbf{k}, \omega). \quad (17)$$

By integrating over the frequency in Eq. (16), it is easy to see that the rf spectrum or Raman spectrum is normalized to the impurity density, i.e., $\int d\omega I(\omega) = n_{\text{imp}}$. In the following, we always plot a normalized spectrum by dividing $I(\omega)$ by n_{imp} . It is also useful to note that, to calculate the rf spectrum or Raman spectrum one needs to integrate the spectral function over different momenta. As a result, a clear interpretation of the spectroscopic measurement, in terms of the zero-momentum spectral function, may become difficult. In Appendix B, we briefly discuss the spectral function of a unitary Fermi polaron at finite momentum predicted by the two T -matrix theories.

A. rf spectrum

In Fig. 6, we show the rf spectra of a unitary Fermi polaron at two temperatures, $T = 0.2T_F$ [Fig. 6(a)] and $T = 0.5T_F$

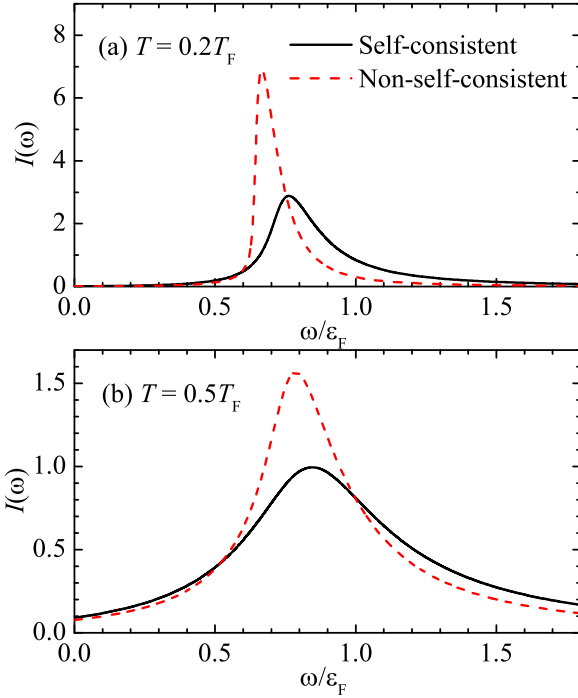


FIG. 6. The ejection rf spectra of a unitary Fermi polaron at (a) $T = 0.2T_F$ and (b) $T = 0.5T_F$, in units of ϵ_F^{-1} . The black solid lines and red dashed lines report the predictions of the self-consistent and non-self-consistent many-body T -matrix theories, respectively. Here, we use impurity density $n_{\text{imp}} = 0.1n$. The spectrum is normalized, so $\int d\omega I(\omega) = 1$.

[Fig. 6(b)]. In each spectrum, there is a peak associated with the attractive polaron. The peak position is located at $\omega \simeq -\mathcal{E}_P$, while the peak width might become broader than the decay rate of the zero-momentum attractive polaron due to the contribution from finite-momentum Fermi polarons. We observe that the self-consistent many-body T -matrix theory predicts a broader rf peak at higher energy than the non-self-consistent theory. This is consistent with what we find in the spectral function.

The changes due to the self-consistent treatment are quantitatively significant, as the height of the rf peak is much reduced. For example, at the low temperature $T = 0.2T_F$, the rf peak height can be reduced by a factor of more than 2. As temperature increases, the reduction effect becomes weaker. At $T = 0.5T_F$, we can see a reduction of only about 35%.

At this point, it is interesting to compare the theoretical predictions of the two T -matrix theories with the latest rf measurement from the Massachusetts Institute of Technology (MIT) at $T < T_F$, as shown in Fig. 7. To simulate the realistic experimental conditions, we have taken a convolution of the theoretical rf spectrum with a Lorentzian line shape, which accounts for the experimental energy resolution of $0.1\epsilon_F$. We have also horizontally shifted the spectrum by an amount of $0.09\epsilon_F$ to compensate for the final-state effect arising from the residual interaction of the impurity in the second hyperfine state after transfer. Otherwise, there are no free adjustable parameters used in the comparison. A more refined treatment of the final-state effect will be explored in future studies.

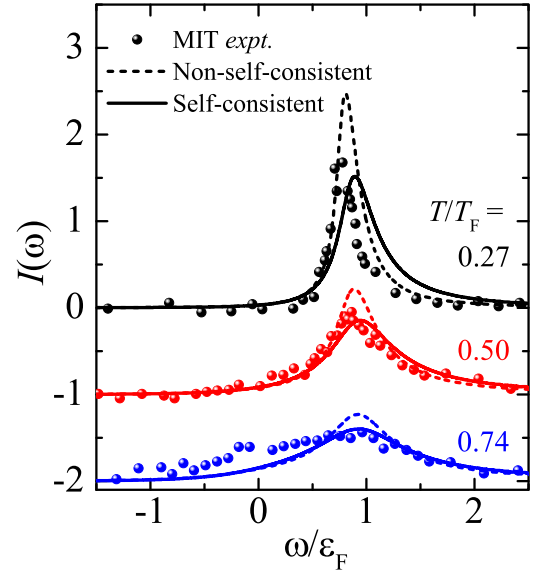


FIG. 7. The ejection rf spectra, predicted by the self-consistent (solid lines) and non-self-consistent (dashed lines) many-body T -matrix theories, are compared with the experimental data from MIT (circles) [15]. Here, we use impurity density $n_{\text{imp}} = 0.1n$. We have applied a Lorentzian broadening on all the theoretical curves to take into account a well-calibrated experimental energy resolution of $0.1\epsilon_F$ and have also shifted the curves to the right by $0.09\epsilon_F$ in order to eliminate the residual final-state effect.

It is readily seen that, overall, the predictions from the self-consistent many-body T -matrix theory better fit the experimental data. The non-self-consistent theory always predicts a higher peak height than the experimental observation. It is worth noting that, as temperature increases, a pronounced peak starts to emerge at about $\omega \sim 0$ in the measured rf spectrum. However, both T -matrix theories fail to produce such an important experimental feature. As a result, at $T = 0.74T_F$ we find an apparent discrepancy between theory and experiment near the zero frequency (see the bottom curves and data in Fig. 7 at $\omega \sim 0$).

This discrepancy becomes particularly evident when we compare the results for the peak position (which is interpreted as $-\mathcal{E}_P$) and the FWHM width (i.e., the decay rate Γ of the polaron in our interpretation), which are extracted from the simulated theoretical curves and the measured rf spectra. These results are shown in Figs. 8(a) and 8(b), respectively. We see a clear jump in the measured peak position at temperature $T \sim 0.8T_F$. Above this temperature, the peak position seems to be pinned near zero frequency. In contrast, the peak position predicted by both T -matrix theories gradually decreases towards $\omega = 0$. In line with the sudden jump in the peak position, the measured FWHM width reaches maximum at $T \sim 0.8T_F$. After this temperature, the width quickly decreases. This observation also cannot be understood by both T -matrix theories. As temperature increases, maximum widths occur at $T \sim 1.2T_F$ and $T \sim 1.5T_F$ for the self-consistent and non-self-consistent calculations, respectively. Moreover, the predicted temperature dependence of the FWHM width appears to be much smoother than what was observed in the measured spectra.

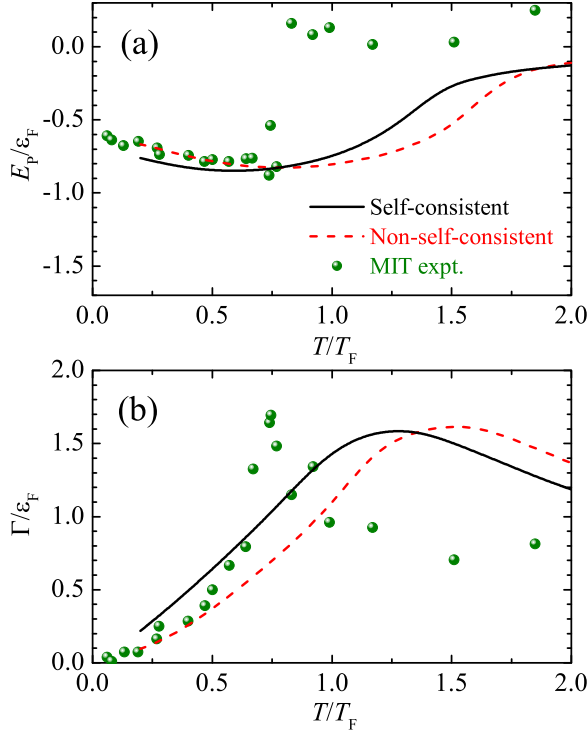


FIG. 8. The peak position and the FWHM width of the ejection rf spectra, predicted by the self-consistent (black solid lines) and non-self-consistent (red dashed lines) many-body T -matrix theories, are compared with the experimental data from MIT (green circles) [15]. Here, we use impurity density $n_{\text{imp}} = 0.1n$ in the calculations of the ejection rf spectra. In the experimental data, we subtracted the energy resolution $0.1\epsilon_F$ in the FWHM width Γ and compensated the final-state energy shift $0.09\epsilon_F$ in the extracted peak position $-\mathcal{E}_p$ [15].

B. Raman spectrum

Finally, let us briefly discuss the Raman spectroscopy. In Fig. 9, we report the Raman spectrum of a unitary Fermi

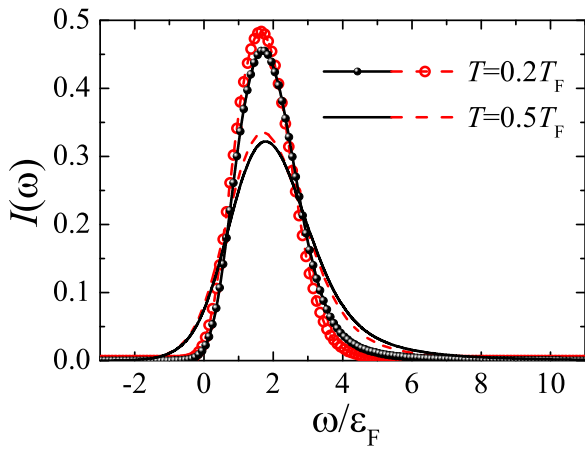


FIG. 9. The ejection Raman spectra of a unitary Fermi polaron at $T = 0.2T_F$ (the lines with symbols) and $T = 0.5T_F$ (plain lines), in units of ϵ_F^{-1} . The black solid lines and red dashed lines report the predictions of the self-consistent and non-self-consistent many-body T -matrix theories, respectively. Here, we use transferred momentum $q = k_F$ and impurity density $n_{\text{imp}} = 0.15n$.

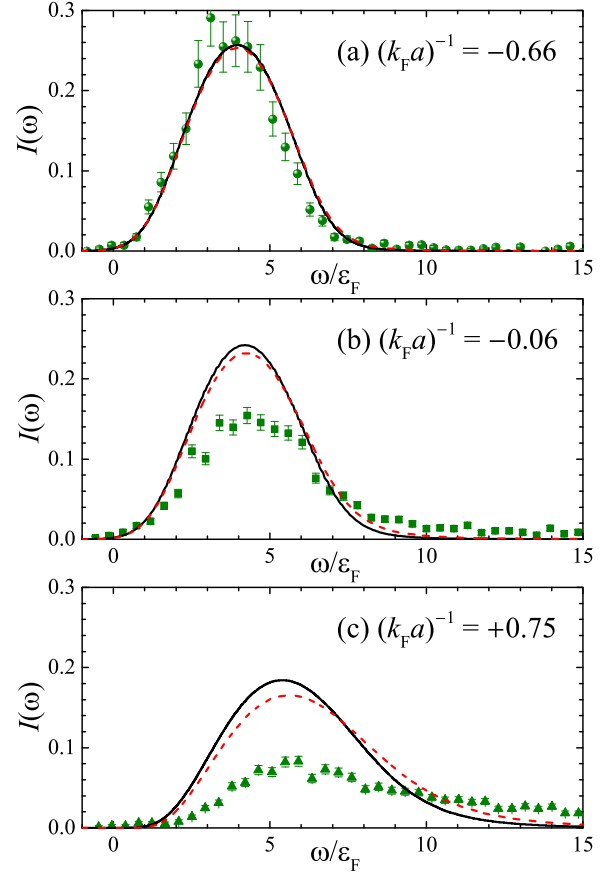


FIG. 10. The ejection Raman spectra, predicted by the self-consistent (black solid lines) and non-self-consistent (red dashed lines) many-body T -matrix theories, are compared with the experimental data from TIIT (symbols) at three different interaction strengths [17]. Here, we use impurity density $n_{\text{imp}} = 0.23n$ and transferred momentum $Q = 1.9k_F$, as in the experiment. The temperature is set to $T = 0.2T_F$. In the theoretical calculations, we do not include the inhomogeneous density profiles due to external harmonic traps, which lead to only small, unimportant changes in the predicted Raman spectrum [31].

polaron at two temperatures, $T = 0.2T_F$ and $T = 0.5T_F$, calculated using both T -matrix theories. At both temperatures, the self-consistency treatment does not lead to notable changes. This probably can be understood from the fact that the Raman spectrum at a large transferred momentum $Q \sim k_F$ is mainly contributed by Fermi polarons at finite momentum with $k \sim k_F$, for which the self-consistency in the impurity Green's function becomes less important.

In Fig. 10, we compare the predictions of the two T -matrix theories with the latest measurement of the Raman spectrum from the Technion-Israel Institute of Technology (TIIT) at a temperature around $0.2T_F$. For a weak interaction between the impurity and the Fermi sea in Fig. 10(a), the predicted Raman spectra from the two T -matrix theories are indistinguishable at the scale of the figure. Both predictions agree well with the measured spectrum. For large interaction strengths, near the unitary limit [Fig. 10(b)] or on the BEC side of the Feshbach resonance [Fig. 10(c)], the two T -matrix theories do predict different theoretical Raman spectra. However, the improvement due to the self-consistency treatment seems to

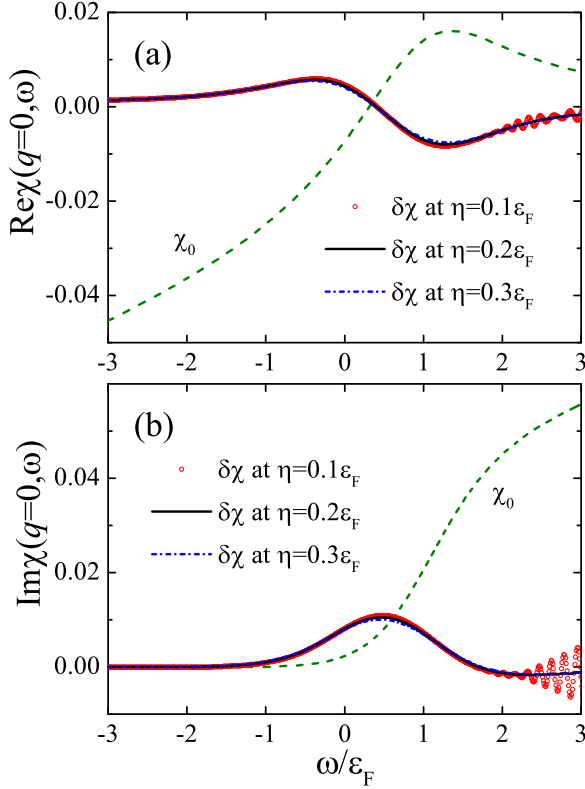


FIG. 11. The real part and imaginary part of the pair propagator $\chi_0(q, \omega) = \Gamma_0^{-1}(q, \omega)$ and $\delta\chi(q, \omega)$ at zero wave vector $q = 0$, in arbitrary units. The red circles, black solid lines, and blue dot-dashed lines show the results with $\eta/\varepsilon_F = 0.1, 0.2$, and 0.3 , respectively. We consider the unitary limit and temperature $T = 0.2T_F$.

be too small to resolve the puzzling discrepancy found earlier between the non-self-consistent T -matrix theoretical results and the experimental observations [31].

V. CONCLUSIONS AND OUTLOOKS

In conclusion, we studied the spectral function of Fermi polarons at finite temperature in three dimensions by applying

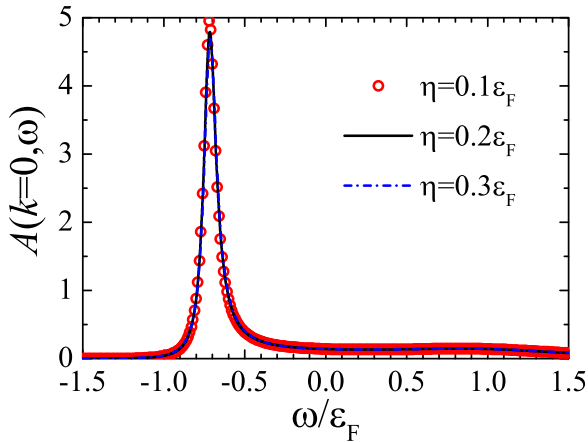


FIG. 12. The zero-momentum spectral function, in units of ε_F^{-1} , calculated with $\eta/\varepsilon_F = 0.1$ (red circles), 0.2 (black solid line), and 0.3 (blue dot-dashed line). We consider the unitary limit and temperature $T = 0.2T_F$.

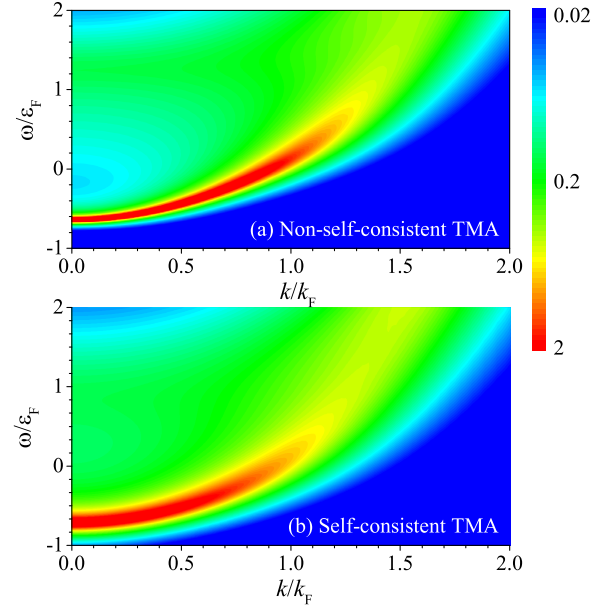


FIG. 13. The contour plot of the impurity spectral function $A(k, \omega)$ of a unitary Fermi polaron at $T = 0.2T_F$ as a function of momentum k and frequency ω , predicted by (a) the non-self-consistent and (b) self-consistent many-body T -matrix theories. The two-dimensional plot is shown at a logarithmic scale in units of ε_F^{-1} , as indicated by the color bar.

a self-consistent many-body T -matrix theory. In comparison with the widely used non-self-consistent T -matrix theory [23,28,29], we find the introduction of the self-consistency in the impurity Green's function quantitatively changes the polaron spectral function. The changes are mostly significant at low temperature, where the self-consistency treatment increases the polaron decay rate and therefore notably broadens the line shape of the spectral function. We related the enhanced polaron decay rate to the two-particle vertex function, which describes the in-medium molecule state created by the successive scatterings between the impurity and the Fermi sea.

Although we believe that the molecule state is more accurately described by the self-consistent many-body T -matrix theory, there is no consensus that the self-consistency in the impurity Green's function will necessarily improve the description of Fermi polarons. Therefore, we compared the theoretical predictions from both self-consistent and non-self-consistent theories with the latest experimental measurements [15,17]. For the radio-frequency spectroscopy of a unitary Fermi polarons [15], at low temperature (i.e., below $0.8T_F$) we observed that the self-consistent T -matrix theory seems to explain better the experimental data. However, at high temperature, both T -matrix theories fail to account for the experimental observations. For the Raman spectroscopy of Fermi polarons [17], the use of the self-consistent T -matrix theory does not lead to too much of a difference. Near the Feshbach resonance, the predictions of both T -matrix theories differ largely from the experimental results at $T \sim 0.2T_F$. The discrepancy between the T -matrix theories and experiments for both radio-frequency spectroscopy and Raman spectroscopy suggests that we need to significantly improve

the theory of the polaron spectral function, beyond the standard T -matrix approximation.

Alternatively, we may consider the case of heavy Fermi polarons, for which the exact solution can be obtained by using a functional-determinant approach [6,7]. The exact spectral function of heavy polarons in a BCS Fermi superfluid was recently determined [38,39]. It would be interesting to calculate the spectral function of such heavy BCS polarons with both self-consistent and non-self-consistent many-body T -matrix theories and compare the approximate results with the exact solution. Finally, it might be useful to note that our technique used to calculate a dressed Green's function in the real frequency could be extended to investigate the spectral function of other interacting Fermi systems, particularly a two-component spin-1/2 Fermi gas with a balanced population in each component.

ACKNOWLEDGMENT

This research was supported by the Australian Research Council's (ARC) Discovery Program, Grants No. DP240101590 (H.H.) and No. DP240100248 (X.-J.L.).

APPENDIX A: THE η DEPENDENCE OF THE DIFFERENCE IN THE VERTEX FUNCTION

Throughout this work, in the calculation of the difference in the vertex function $\delta\chi \equiv \Gamma^{-1} - \Gamma_0^{-1}$, we have added a small imaginary part $\eta = 0.2\varepsilon_F$ to the frequency ω in order to

remove the singularity in the integrand of Eq. (7). In Fig. 11, we show the dependence of $\delta\chi(q=0, \omega)$ at zero momentum on the choice of the value η in comparison with the dominant contribution $\chi_0 = \Gamma_0^{-1}(q=0, \omega)$. Here, as an example, we consider the unitary limit at temperature $T = 0.2T_F$. At the scale of Γ_0^{-1} , we can barely see the changes in $\delta\chi$ due to the use of different values of η . We find that the use of a smaller value of $\eta = 0.1\varepsilon_F$ introduces an oscillation at large frequency. This is anticipated since the integrand needs to be more finely sampled in our Gaussian quadrature integration, which is time-consuming. Our choice of $\eta = 0.2\varepsilon_F$ turns to be a good balanced selection, so the numerical calculations can be carried out in an efficient and accurate way. In Fig. 12, we also report the corresponding spectral functions at different values of η . The three spectral functions are indistinguishable from each other.

APPENDIX B: SPECTRAL FUNCTION AT FINITE MOMENTUM

In Fig. 13, we present the polaron spectral function at finite momentum in the form of a two-dimensional contour plot. We consider the unitary limit with $1/(k_F a) = 0$ and temperature $T = 0.2T_F$. We find that in comparison with the non-self-consistent T -matrix results in Fig. 13(a), the self-consistency treatment in Fig. 13(b) leads to a much broader polaron peak. As the momentum increases, it also makes the polaron easier to dissolve.

-
- [1] L. D. Landau, Electron motion in crystal lattices, *Phys. Z. Sowjetunion* **3**, 664 (1933).
 - [2] A. S. Alexandrov and J. T. Devreese, *Advances in Polaron Physics*, Springer Series in Solid-State Sciences Vol. 159 (Springer, New York, 2010).
 - [3] F. Chevy, Universal phase diagram of a strongly interacting Fermi gas with unbalanced spin populations, *Phys. Rev. A* **74**, 063628 (2006).
 - [4] A. Schirotzek, C.-H. Wu, A. Sommer, and M. W. Zwierlein, Observation of Fermi polarons in a tunable Fermi liquid of ultracold atoms, *Phys. Rev. Lett.* **102**, 230402 (2009).
 - [5] P. Massignan, M. Zaccanti, and G. M. Bruun, Polarons, dressed molecules and itinerant ferromagnetism in ultracold Fermi gases, *Rep. Prog. Phys.* **77**, 034401 (2014).
 - [6] R. Schmidt, M. Knap, D. A. Ivanov, J.-S. You, M. Cetina, and E. Demler, Universal many-body response of heavy impurities coupled to a Fermi sea: A review of recent progress, *Rep. Prog. Phys.* **81**, 024401 (2018).
 - [7] J. Wang, Functional determinant approach investigations of heavy impurity physics, *AAPPS Bull.* **33**, 20 (2023).
 - [8] H. Tajima, H. Moriya, W. Horiuchi, E. Nakano, and K. Iida, Intersections of ultracold atomic polarons and nuclear clusters: How is a chart of nuclides modified in dilute neutron matter? *AAPPS Bull.* **34**, 9 (2024).
 - [9] I. Bloch, J. Dalibard, and W. Zwerger, Many-body physics with ultracold gases, *Rev. Mod. Phys.* **80**, 885 (2008).
 - [10] C. Chin, R. Grimm, P. Julienne, and E. Tiesinga, Feshbach resonances in ultracold gases, *Rev. Mod. Phys.* **82**, 1225 (2010).
 - [11] Y. Zhang, W. Ong, I. Arakelyan, and J. E. Thomas, Polaron-to-polaron transitions in the radio-frequency spectrum of a quasi-two-dimensional Fermi gas, *Phys. Rev. Lett.* **108**, 235302 (2012).
 - [12] C. Kohstall, M. Zaccanti, M. Jag, A. Trenkwalder, P. Massignan, G. M. Bruun, F. Schreck, and R. Grimm, Metastability and coherence of repulsive polarons in a strongly interacting Fermi mixture, *Nature (London)* **485**, 615 (2012).
 - [13] M. Koschorreck, D. Pertot, E. Vogt, B. Fröhlich, M. Feld, and M. Köhl, Attractive and repulsive Fermi polarons in two dimensions, *Nature (London)* **485**, 619 (2012).
 - [14] F. Scazza, G. Valtolina, P. Massignan, A. Recati, A. Amico, A. Burchianti, C. Fort, M. Inguscio, M. Zaccanti, and G. Roati, Repulsive Fermi polarons in a resonant mixture of ultracold ${}^6\text{Li}$ atoms, *Phys. Rev. Lett.* **118**, 083602 (2017).
 - [15] Z. Yan, P. B. Patel, B. Mukherjee, R. J. Fletcher, J. Struck, and M. W. Zwierlein, Boiling a unitary Fermi liquid, *Phys. Rev. Lett.* **122**, 093401 (2019).
 - [16] M. Cetina, M. Jag, R. S. Lous, I. Fritsche, J. T. M. Walraven, R. Grimm, J. Levinsen, M. M. Parish, R. Schmidt, M. Knap, and E. Demler, Ultrafast many-body interferometry of impurities coupled to a Fermi sea, *Science* **354**, 96 (2016).
 - [17] G. Ness, C. Shkedorov, Y. Florshaim, O. K. Diessel, J. von Milczewski, R. Schmidt, and Y. Sagi, Observation of a smooth polaron-molecule transition in a degenerate Fermi gas, *Phys. Rev. X* **10**, 041019 (2020).
 - [18] X. Cui and H. Zhai, Stability of a fully magnetized ferromagnetic state in repulsively interacting

- ultracold Fermi gases, *Phys. Rev. A* **81**, 041602(R) (2010).
- [19] M. M. Parish and J. Levinsen, Highly polarized Fermi gases in two dimensions, *Phys. Rev. A* **87**, 033616 (2013).
- [20] W. E. Liu, J. Levinsen, and M. M. Parish, Variational approach for impurity dynamics at finite temperature, *Phys. Rev. Lett.* **122**, 205301 (2019).
- [21] W. E. Liu, Z.-Y. Shi, M. M. Parish, and J. Levinsen, Theory of radio-frequency spectroscopy of impurities in quantum gases, *Phys. Rev. A* **102**, 023304 (2020).
- [22] H. Hu, J. Wang, R. Lalor, and X.-J. Liu, Two-dimensional coherent spectroscopy of trion-polaritons and exciton-polaritons in atomically thin transition metal dichalcogenides, *AAPPS Bull.* **33**, 12 (2023).
- [23] R. Combescot, A. Recati, C. Lobo, and F. Chevy, Normal state of highly polarized Fermi gases: Simple many-body approaches, *Phys. Rev. Lett.* **98**, 180402 (2007).
- [24] H. Hu, B. C. Mulkerin, J. Wang, and X.-J. Liu, Attractive Fermi polarons at nonzero temperatures with a finite impurity concentration, *Phys. Rev. A* **98**, 013626 (2018).
- [25] H. Tajima and S. Uchino, Many Fermi polarons at nonzero temperature, *New J. Phys.* **20**, 073048 (2018).
- [26] J. Wang, X.-J. Liu, and H. Hu, Roton-induced Bose polaron in the presence of synthetic spin-orbit coupling, *Phys. Rev. Lett.* **123**, 213401 (2019).
- [27] B. C. Mulkerin, X.-J. Liu, and H. Hu, Breakdown of the Fermi polaron description near Fermi degeneracy at unitarity, *Ann. Phys. (NY)* **407**, 29 (2019).
- [28] H. Tajima and S. Uchino, Thermal crossover, transition, and coexistence in Fermi polaronic spectroscopies, *Phys. Rev. A* **99**, 063606 (2019).
- [29] H. Hu and X.-J. Liu, Fermi polarons at finite temperature: Spectral function and rf spectroscopy, *Phys. Rev. A* **105**, 043303 (2022).
- [30] H. Hu, J. Wang, J. Zhou, and X.-J. Liu, Crossover polarons in a strongly interacting Fermi superfluid, *Phys. Rev. A* **105**, 023317 (2022).
- [31] H. Hu and X.-J. Liu, Raman spectroscopy of Fermi polarons, *Phys. Rev. A* **106**, 063306 (2022).
- [32] H. Hu, J. Wang, and X.-J. Liu, Thermally stable p -wave repulsive Fermi polaron without a two-body bound state, *AAPPS Bull.* **33**, 27 (2023).
- [33] N. Prokof'ev and B. Svistunov, Fermi-polaron problem: Diagrammatic Monte Carlo method for divergent sign-alternating series, *Phys. Rev. B* **77**, 020408(R) (2008).
- [34] J. Vlietinck, J. Ryckebusch, and K. Van Houcke, Quasiparticle properties of an impurity in a Fermi gas, *Phys. Rev. B* **87**, 115133 (2013).
- [35] P. Kroiss and L. Pollet, Diagrammatic Monte Carlo study of a mass-imbalanced Fermi-polaron system, *Phys. Rev. B* **91**, 144507 (2015).
- [36] O. Goulko, A. S. Mishchenko, N. Prokof'ev, and B. Svistunov, Dark continuum in the spectral function of the resonant Fermi polaron, *Phys. Rev. A* **94**, 051605(R) (2016).
- [37] M. Knap, A. Shashi, Y. Nishida, A. Imambekov, D. A. Abanin, and E. Demler, Time-dependent impurity in ultracold fermions: Orthogonality catastrophe and beyond, *Phys. Rev. X* **2**, 041020 (2012).
- [38] J. Wang, X.-J. Liu, and H. Hu, Exact quasiparticle properties of a heavy polaron in BCS Fermi superfluids, *Phys. Rev. Lett.* **128**, 175301 (2022).
- [39] J. Wang, X.-J. Liu, and H. Hu, Heavy polarons in ultracold atomic Fermi superfluids at the BEC-BCS crossover: Formalism and applications, *Phys. Rev. A* **105**, 043320 (2022).
- [40] R. Haussmann, Properties of a Fermi liquid at the superfluid transition in the crossover region between BCS superconductivity and Bose-Einstein condensation, *Phys. Rev. B* **49**, 12975 (1994).
- [41] X.-J. Liu and H. Hu, Self-consistent theory of atomic Fermi gases with a Feshbach resonance at the superfluid transition, *Phys. Rev. A* **72**, 063613 (2005).
- [42] H. Hu, X.-J. Liu, and P. D. Drummond, Comparative study of strong-coupling theories of a trapped Fermi gas at unitarity, *Phys. Rev. A* **77**, 061605(R) (2008).
- [43] Q. Chen, J. Stajic, S. Tan, and K. Levin, BCS-BEC crossover: From high temperature superconductors to ultracold superfluids, *Phys. Rep.* **412**, 1 (2005).
- [44] S. Tsuchiya, R. Watanabe, and Y. Ohashi, Single-particle properties and pseudogap effects in the BCS-BEC crossover regime of an ultracold Fermi gas above T_c , *Phys. Rev. A* **80**, 033613 (2009).
- [45] R. Haussmann, M. Punk, and W. Zwerger, Spectral functions and rf response of ultracold fermionic atoms, *Phys. Rev. A* **80**, 063612 (2009).
- [46] F. Palestini, A. Perali, P. Pieri, and G. C. Strinati, Dispersions, weights, and widths of the single-particle spectral function in the normal phase of a Fermi gas, *Phys. Rev. B* **85**, 024517 (2012).
- [47] E. J. Mueller, Review of pseudogaps in strongly interacting Fermi gases, *Rep. Prog. Phys.* **80**, 104401 (2017).
- [48] X. Li, S. Wang, X. Luo, Y.-Y. Zhou, K. Xie, H.-C. Shen, Y.-Z. Nie, Q. Chen, H. Hu, Y.-A. Chen, X.-C. Yao, and J.-W. Pan, Observation and quantification of pseudogap in unitary Fermi gases, *Nature (London)* **626**, 288 (2024).
- [49] L. N. Cooper, Bound electron pairs in a degenerate Fermi gas, *Phys. Rev.* **104**, 1189 (1956).
- [50] M. Punk, P. T. Dumitrescu, and W. Zwerger, Polaron-to-molecule transition in a strongly imbalanced Fermi gas, *Phys. Rev. A* **80**, 053605 (2009).